# Supporting Information

**Correlating Miscibility, Mechanical Parameters, and Stability of Ternary Polymer Blends for High-Performance Solar Cells**

*Kangkang Zhou,[a] Kaihu Xian,[a] Ruijie Ma,[b] Junwei Liu,[a] Mengyuan Gao,[a] Saimeng Li,[a] Tao Liu,[c] Yu Chen,[d] Yanhou Geng,[a,e] Long Ye *[a]*

[a]School of Materials Science and Engineering, Tianjin Key Laboratory of Molecular Optoelectronic Sciences, Tianjin University, Collaborative Innovation Center of Chemical Science and Engineering (Tianjin), Tianjin 300350, China

[b]Department of Electronic and Information Engineering, Research Institute for Smart Energy (RISE), The Hong Kong Polytechnic University, Hung Hom, Kowloon, Hong Kong, 999077, China

[c]School of Resources, Environments and Materials, Guangxi University, Nanning 530004, China

[d]Institute of High Energy Physics, Chinese Academy of Sciences, Beijing 100049, China

[e]Joint School of National University of Singapore and Tianjin University, International Campus of Tianjin University Binhai New City, Fuzhou, Fujian, 350207 China

*Correspondence: yelong@tju.edu.cn

Experimental Section

Materials. All chemicals were purchased from commercial sources without further purification. PM6, PTQ10, PTVT-T, PY-IT and PNDI were purchased from Solarmer Materials Inc. PYF-IT and PNDIT-F3N were purchased from eFlexPV Limited. PEDOT:PSS (4083) was purchased from the CleviosTM. PPCBMB was provided by Tao Liu's group. All solvents were purchased from Sigma Aldrich , Energy Chemical or Heowns.

Device Fabrication. The conventional device structure of Substrate/ PEDOT:PSS/ active layer/ PNDIT-F3N/ Ag was adopted in this study. The rigid device is made on a ITO glass substrate, while the flexible device is on a PET substrate. PM6:PYF-IT, PM6:PYF-IT:PTQ10, PM6:PYF-IT:PTVT-T, PM6:PYF-IT:PNDI blends were dissolved in chloroform at the total concentration of 14 mg/mL and the optimal D/A ratio was 1:1.2 (w/w). The blend solutions were stirred at 60 °C for 4 h to fully dissolve. Prior to spin-coating the active layer solutions, 2% CN (v/v) was added
into the solutions. The PM6:PY-IT blends (1:1 weight ratio), were dissolved in o-XY (the concentration of donor was 10/11/12/13/14/15 mg mL-1 for all blends with the increase of PPCBMB's content), with 1% vol 1-chloronaphthalene as additive (1 vol%).PNDIT-F3N was dissolved in methanol at the concentration of 0.5 mg/mL with 0.5 v% of acetic acid. Devices were fabricated as follows. First, ITO substrates were treated with UV ozone for 25 min. Then, about 20 nm PEDOT:PSS layers were deposited via spin-coating on the pre-cleaned ITO substrates and annealed at 150 °C for 20 min. Subsequently, the substrates were transferred to the argon-filled glove box. The mixed solutions were spin-coated onto the PEDOT:PSS layers, and the thicknesses of all active layers were about 100 nm. Note that the 0%, 17%, and 33% mixed solutions wereThen the films were treated with thermal annealing at 100 °C for 10 min. PNDIT-F3N was spin-coated on the top of the active layers. Finally, 100 nm thick Ag was deposited on the top of PNDIT-F3N layer under high vacuum. The fabrication process of flexible devices is exactly the same as that of rigid devices. The effective area of the

small area cells is about 0.04 cm$^2$. Thin-films were prepared by spin coating from the toluene solutions.

Electrochemical Properties. The J-V measurements were performed via the AAA solar simulator (SS-F5-3A, Enli Technology Co. Ltd, Taiwan) along with AM 1.5G spectra whose intensity was calibrated by the certified standard silicon solar cell at 100 mW/cm$^2$. The EQE spectra were measured through the Solar Cell Spectral Response Measurement System QE-R3011 (Enli Technology Co. Ltd, Taiwan). The thickness of blend layer was measured via the surface profilometer Bruker Dektak XT.

GIWAXS Characterizations. The samples for GIWAXS measurements were prepared on silicon substrates and the conditions were the same as the device preparation. GIWAXS experiments were carried out at the beamline 1W1A of Beijing Synchrotron Radiation Facility (BSRF) with an incident beam energy at 8 keV and the beamline BL16B1, BL14B1 and BL02U2 of Shanghai Synchrotron Radiation Facility (SSRF) with an incident beam energy at 10 keV. Scattering data were all collected with a fixed grazing angle of 0.2°. The beam center and sample-to-detector distance were calibrated with LaB6.

Morphology Characterizations. The surface morphology of films was measured by a Nanoscope V AFM (Bruker Multimode 8) in tapping mode. The type of AFM cantilever is RTESPA-300, which possesses a k constant of about 40 N/m. The scanning area was 2 μm × 2 μm and the resolution is 256×256 pixels. The TEM images of films were obtained by the JEOL JEM-2100PLUS electron microscope and its accelerating voltage is 200 kV. The magnification of all TEM images is 30K.

Mechanical measurements. FOE tests were carried out using a polarizing microscope (ECLIPSE LV100N POL, Nikon) and a custom-designed tensile stage. The films were coated on glasses (size: 1.7 ×1.7 cm) and then transferred to the PDMS film via water. The crack-onset strains of films were measured by stretching PDMS until the films

started to crack under the observation of a polarized light microscope. Stress-strain curves were acquired using a custom-designed FOW instrument (Auto Tensile Tester, MTM 920, SYSTESTER). In the FOW test, the blend films were coated on precleaned glasses (size: 2 × 2 cm) and then cut into a rectangle shape and transferred to the water surface. The blend films were moved above the PDMS fixture and then glued to the PDMS by lowering the liquid level. The thickness of the neat and blend films is about 100 nm.

The elastic modulus of the film is obtained from the wavelength of the surface crease produced when the film on the elastic substrate releases the pre-tightened elastic substrate.

$$E_f = 3E_s\left(\frac{1-v_f^2}{1-v_s^2}\right)\left(\frac{\lambda_b}{2\pi d_f}\right)^3$$

eq (S1)

where $v_s$ is the Poisson ratio of substrate, $\lambda_b$ is the buckling wavelength, $v_f$ is the Poisson ratio of the thin film, $E_s$ is the elastic modulus of the elastomer substrate and $d_f$ is the thin film thickness.

In the FOE method, the adhesion and elastic mismatch between the film and the substrate affect the deformation and fracture behavior of the film, so the elastic modulus and crack initiation strain can depend on the characteristics of the substrate. The elastic modulus obtained by the FOW method has little influence on the substrate (water), which can reflect the real fracture behavior and elastic modulus. Therefore, the elastic modulus obtained by FOE is different from that obtained by FOW, but the change trend is similar.

The Davies model predicts the blending of interpenetrating network structures well, and its equation is as follows:[1]

$$E_i = \left[V_1 E_1^{1/5} + V_2 E_2^{1/5}\right]^5$$

eq (S2)

Where $V$ and $E$ represent the volume fraction and elastic modulus, respectively. In previous work, we demonstrated that the PM6: PY-IT binary blend has an excellent correlation with Davies model. Thus, we express the elastic modulus of PM6:PYF-

IT/PY-IT blend as $E_i$, which varies with the third components. The Kerner model is widely used to predict polymer blends of immiscible components (i.e., dispersed-continuous phase morphology).[2] The equation is as follows:

$$E = \left[\gamma - \frac{(1 - V_3)E_3 + \beta(\alpha + V_3)E_i}{(1 + \alpha V_3)E_3 + \alpha\beta(1 - V_3)E_i}\right]E_i \qquad \text{eq (S3)}$$

$$\beta = \frac{1 + v_m}{1 + v_i}, \; \gamma = \frac{1 + v}{1 + v_m}, \; \alpha = \frac{2(4 - 5v_m)}{7 - 5v_m}$$

Where $v$, $m$, and $i$ represent Poisson's ratio, continuous and dispersed phase, respectively. PTQ10 is immiscible with PM6 and PYF-IT, forming obvious dispersed phase morphology, so the PTQ10 blends can be predicted by Kerner-Davies model. Halpin-Tsai model is an equation considering polymer geometry,[3,4] which is widely used to predict the elastic modulus of bulk and spherical blends, which can be expressed as equation:

$$E = E_m\left(\frac{1 + \zeta_1\eta_1 V_1 + \zeta_2\eta_2 V_2}{1 - \eta_1 V_1 - \eta_2 V_2}\right) \qquad \text{eq (S4)}$$

$$\eta_1 = \frac{E_1/E_m - 1}{E_1 E_m + \zeta_1}, \eta_2 = \frac{E_2/E_m - 1}{E_2 E_m + \zeta_2}$$

Where $\zeta_i$ and $m$ represent the shape factor of fillers and matrix. Since PY-IT and PPCBMB are short fibers in the blend membrane, their $\zeta$ value is assumed to be 13.3, similar to the previous study. We found that the experimental data were close to the Halpin-Tsai model, and results showed that the elastic modulus of the PPCBMB ternary blend system was also predictable.

Since PTVT-T is miscible with PM6 and PYF-IT and has little influence on the aggregation, we developed the Davies model in the ternary blending. The equation is as follows:

$$E^{1/5} = V_1 E_1^{1/5} + V_2 E_2^{1/5} + V_3 E_3^{1/5} \qquad \text{eq (S5)}$$

Davies model is consistent with the variation trend of the elastic modulus of PTVT-T ternary blends, and the relationship between the elastic modulus and the content of PTVT-T is well predicted. The Coran-Patel model describes the elastic modulus

variation of the blending of soft and hard materials,[5,6] and Ye et al.[7] used this model to predict various SEBS ternary blend systems. In PNDI blends, PNDI with high stretchability and low elastic modulus can act as soft phase, thus Coran-Patel and Davies models can be combined to describe these blends. The equation is as follows:

$$E = \left(1 - V_3^n\right)\left(nV_3 + 1\right)\left(E_u - E_l\right) + E_l \qquad \text{eq (S6)}$$

$$E_u = E_i\left(1 - V_3\right) + E_3V_3$$

$$E_l = \frac{E_iE_3}{E_3\left(1 - V_3\right) + E_iV_3}$$

Where $E_i$ is the elastic modulus of PM6:PYF-IT, and $n$ represents the adjustable parameter, which is related to the degree of softness and hardness. Considering the elastic modulus of PNDI and miscible with PYF-IT, $n$ is determined to be 1. When substituting the relevant values, the curve of Coran Patel-Davies model shows excellent agreement with the experimental data.

Table S1 The optimal photovoltaic performance of the polymer solar cells.

| Active layer | The third component content | $V_{oc}$ (mV) | $J_{sc}$ (mA/cm$^2$) | FF (%) | PCE (%) |
|---|---|---|---|---|---|
| PM6:PYF-IT:PTQ10 | 0 | 901 | 23.55 | 70.2 | 15.02 (14.65±0.27) |
| | 0.1 | 905 | 24.01 | 70.1 | 15.23 (14.98±0.19) |
| | 0.2 | 895 | 23.66 | 67.2 | 14.21 (14.08±0.22) |
| | 0.3 | 897 | 21.92 | 66.6 | 13.10 (12.70±0.25) |
| | 0.5 | 874 | 22.33 | 64.6 | 12.62 (12.51±0.21) |
| | 0.7 | 869 | 22.56 | 63.5 | 12.45 (12.18±0.14) |
| | 1 | 846 | 21.01 | 61.9 | 11.00 (10.56±0.23) |
| PM6:PYF-IT:PTVT-T | 0.1 | 898 | 23.82 | 70.6 | 15.10 (14.90±0.20) |
| | 0.2 | 894 | 23.76 | 75.9 | 16.12 (15.92±0.15) |
| | 0.3 | 874 | 23.32 | 73.5 | 14.98 (14.52±0.16) |
| | 0.5 | 856 | 22.42 | 73.0 | 14.01 (14.17±0.19) |
| | 0.7 | 851 | 21.13 | 72.2 | 12.99 (12.76±0.23) |
| | 1 | 828 | 19.40 | 70.3 | 11.23 (10.50±0.52) |
| PM6:PYF-IT:PNDI | 0.1 | 903 | 23.88 | 71.8 | 15.48 (15.32±0.21) |
| | 0.2 | 905 | 23.12 | 69.8 | 14.60 (14.22±0.26) |
| | 0.3 | 908 | 22.00 | 68.2 | 13.61 (13.87±0.15) |
| | 0.5 | 912 | 18.45 | 50.9 | 8.62 (8.58±0.12) |
| | 0.7 | 921 | 15.32 | 43.7 | 6.21 (6.16±0.13) |
| | 1 | 959 | 6.99 | 51.0 | 3.45 (3.42±0.11) |
| PM6:PY-IT :PPCBMB | 0 | 942 | 23.39 | 75.3 | 16.59 (16.34±0.17) |
| | 0.2 | 956 | 24.10 | 78.4 | 18.06 (17.81±0.26) |
| | 0.4 | 961 | 22.74 | 73.0 | 15.95 (15.81±0.18) |
| | 0.6 | 970 | 20.53 | 71.9 | 14.32 (14.12±0.21) |
| | 0.8 | 979 | 16.89 | 68.9 | 11.41 (11.15±0.20) |
| | 1 | 996 | 11.27 | 65.8 | 7.39 (7.27±0.19) |

Table S2 Molecular weight of various polymer donors and acceptors.

| | Mw (kg/mol) | PDI |
|---|---|---|

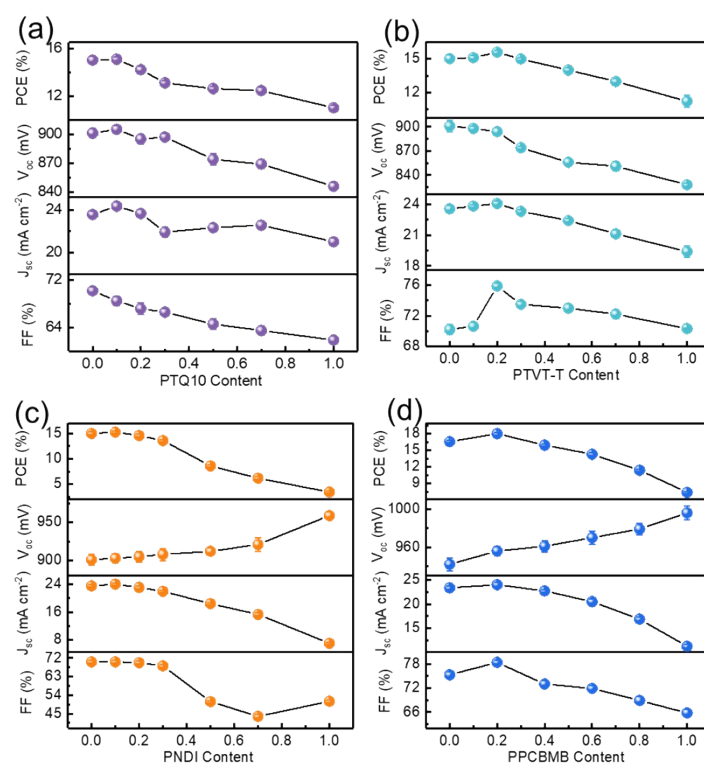| | | |
|---|---|---|
| PM6 | 98.9 | 2.32 |
| PTQ10 | 116.9 | 2.65 |
| PTVT-T | 133.5 | 1.96 |
| PY-IT | 13.7 | 2.01 |
| PYF-IT | 31.1 | 1.40 |
| PNDI | 251.7 | 1.78 |
| PPCBMB | 35.4 | 4.46 |



Figure S1 The photovoltaic performance parameters of ternary polymer solar cells vary with the third components loading. (a)PM6:PYF-IT:PTQ10; (b) PM6:PYF-IT:PTVT-T; (c) PM6:PYF-IT:PNDI; (d) PM6:PY-IT:PPCBMB.

Table S3. The optimal photovoltaic performance of the flexible polymer solar cells.

| Active layers | $V_{oc}$ (mV) | $J_{sc}$ (mA/cm$^2$) | FF (%) | PCE (%) |
|---|---|---|---|---|
| PM6:PYF-IT | 887 | 22.65 | 67.4 | 13.54 |
| PM6:PYF-IT:PTQ10 | 901 | 22.69 | 68.5 | 13.98 |
| PM6:PYF-IT:PTVT-T | 872 | 22.78 | 71.4 | 14.20 |
| PM6:PYF-IT:PNDI | 915 | 22.59 | 68.5 | 14.15 |
| PM6:PY-IT | 925 | 21.15 | 71.3 | 13.95 |
| PM6:PY-IT:PPCBMB | 941 | 22.51 | 73.6 | 15.58 |

Table S4. FOE measured COS and elastic moduli of various polymers.

| | COS (%) | Elastic modulus (GPa) |
|---|---|---|
| PM6 | 15 | 1.13 |
| PTVT-T | 13 | 1.44 |
| PTQ10 | 20 | 2.41 |
| PFY-IT | 6 | 2.31 |
| PY-IT | 5 | 2.65 |
| PNDI | 110 | 0.55 |
| PPCBMB | 9 | 7.52 |

Table S5. PCE and $T_{80}$ lifetime of all-PSCs in previous work and our work.

| Blends | $PCE_{max}$ (%) | Annealing temperature (°C) | $T_{80}$ lifetime ($h$) | Reference |
|---|---|---|---|---|
| PTzBI-Si:N2200 | 11.2 | 80 | ~2000 | [8] |
| PBDTTTPD:N2200 | 6.67 | 150 | ~6 | [9] |
| PBDBT-BV$_{20}$:N2200-TV$_{10}$ | 5.12 | 80 | ~7 | [10] |
| PM6:PYF-T-o (1:1.2 blade) | 9.2 | 70 | ~218 | [11] |

| | | | | |
|---|---|---|---|---|
| PM6:PYF-T-o (1:4 spin) | 5.2 | 70 | ~39 | [11] |
| PM6:PYF-T-o (1:4 blade) | 6.4 | 70 | ~44 | [11] |
| PM6:PF1-TS4 | 8.63 | 85 | ~20 | [12] |
| PBDB-T:P(BDT2BOY5-Cl) | 10.67 | 100 | ~80 | [13] |
| PBDB-T:N2200 | 5.86 | 100 | ~500 | [13] |
| PBDT(T)FTAZ:N2200 | 6.14 | 150 | ~200 | [14] |
| PBDT(T)FTAZ-B5:N2200 | 6.86 | 150 | ~240 | [14] |
| PBDT(T)FTAZ-B5:N2200 (UV 5min) | 6.43 | 150 | ~480 | [14] |
| PBDT(T)FTAZ-B5 N2200 (UV 15min) | 5.78 | 150 | ~320 | [14] |
| PFBZ:N2200 | 8.1 | 150 | ~180 | [15] |
| PBDB-T:PYF-T | 15.68 | 100 | ~145 | [16] |
| PBDB-T:PYF-T:PZT | 16.37 | 100 | ~750 | [16] |
| PM6:PY-IT | 15 | 20~35 | ~2300 | [17] |
| PM6:PY-IT:PYF-IT | 16.6 | 20~35 | ~3600 | [17] |
| PM6: PYF-IT | 15.1 | 20~35 | ~3100 | [17] |
| PM6:PY-V-γ (BC) | 16.6 | 65 | ~1200 | [18] |
| PM6:PY-V-γ (SD) | 17.7 | 65 | ~1400 | [18] |
| PM6:PYF-IT:PTQ10 | 15.23 | 85 | ~2000 | |
| PM6:PYF-IT:PTVT-T | 16.12 | 85 | ~6700 | Our work |
| PM6:PYF-IT:PNDI | 15.48 | 85 | ~8500 | |

| Blends | PCE$_{max}$ (%) | COS (%) | Reference |
|---|---|---|---|
| PM6:PY-IT:PPCBMB | 18.06 | 85 | ~5400 |

Table S6. PCE and COS of all-PSCs in previous work and our work.

| Blends | PCE$_{max}$ (%) | COS (%) | Reference |
|---|---|---|---|
| PBDB-T:P(BDT2BOY5-H) | 8.65 | 19 | [13] |
| PBDB-T:P(BDT2BOY5-F) | 9.64 | 17 | [13] |
| PBDB-T:P(BDT2BOY5-Cl) | 10.67 | 16 | [13] |
| QM-Cl:PY-IT | 17.78 | 7.16 | [19] |
| QM-Cl:PTQ10:PY-IT (0.8:0.2:1.2) | 18.45 | 9.46 | [19] |
| QM-Cl:PTQ10:PY-IT (0.5:0.5:1.2) | 17.06 | 8.57 | [19] |
| QM-Cl:PTQ10:PY-IT (0.2:0.8:1.2) | 16.11 | 5.35 | [19] |
| PTQ10:PY-IT | 13.69 | 3.98 | [19] |
| PBDB-TF:PY-IT | 16.7 | 6.3 | [20] |
| PBQx-TF:PY-IT | 17 | 5.2 | [20] |
| PBQx-TF: PBDB-TF:PY-IT | 18.2 | 5.8 | [20] |
| PM6:PY-IT | 15 | 5.2 | [17] |
| PM6:PY-IT:PYF-IT | 16.6 | 8.1 | [17] |
| PM6: PYF-IT | 15.1 | 6.3 | [17] |
| PBDB-T:PYT-C0 | 4.84 | 2.75 | [21] |
| PBDB-T:PYT-C2 | 11.2 | 12.39 | [21] |

| | | | |
|---|---|---|---|
| PBDB-T:PYT-C4 | 3.37 | 6.03 | [21] |
| PBDB-T:PYT-C8 | 2.74 | 4.77 | [21] |
| PM6:PY-IT | 15.49 | 9.67 | [22] |
| PM6:PYTCl-A | 16.16 | 17.20 | [22] |
| PM6-A: PYTCl-A | 15.54 | 20.01 | [22] |
| PM6-B: PYTCl-A | 14.03 | 18.55 | [22] |
| PM6:PYTCl-B | 13.61 | 18.67 | [22] |
| PM6-A: PYTCl-B | 13.29 | 21.02 | [22] |
| PM6-B: PYTCl-B | 12.73 | 22.74 | [22] |
| PBDB-TF:PY-IT | 15.8 | 5.3 | [23] |
| PQM-Cl:PY-IT | 18 | 6.5 | [23] |
| PTB7-Th: P(NDI2HD-T) | 4.53 | 15.5 | [24] |
| PBDB-T: P(NDI2HD-2T) | 6.89 | 37 | [25] |
| PBDTTTPD:P(NDI2HD-T) | 6.64 | 7.16 | [26] |
| PM6:PYF-IT:PTQ10 | 15.1 | 15.23 | |
| PM6:PYF-IT:PTVT-T | 15.6 | 16.12 | |
| PM6:PYF-IT:PNDI | 15.3 | 15.48 | Our work |
| PM6:PY-IT:PPCBMB | 18.03 | 18.06 | |
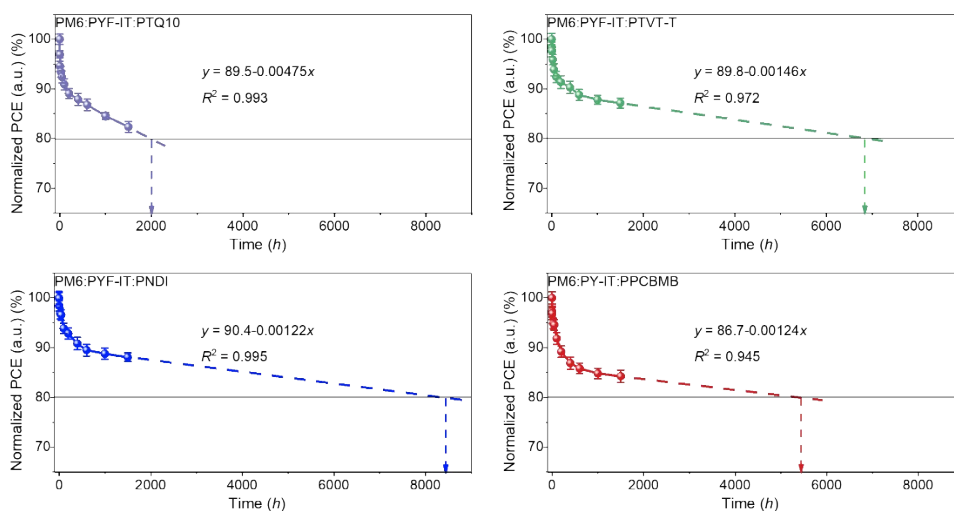
Figure S2. $T_{80}$ analysis of organic solar cells based on PM6:PYF-IT:PTQ10, PM6:PYF-IT:PTVT-T, PM6:PYF-IT:PNDI and PM6:PY-IT:PPCBMB.
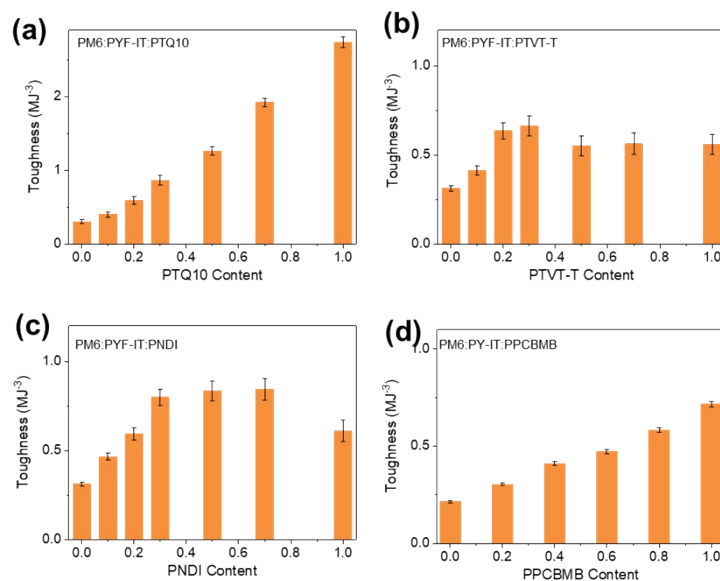


Figure S3. The toughness of various blend films with different blend compositions (FOW): (a) PM6:PYF-IT:PTQ10; (b) PM6:PYF-IT:PTVT-T; (c) PM6:PYF-IT:PNDI; (d) PM6:PY-IT:PPCBMB.
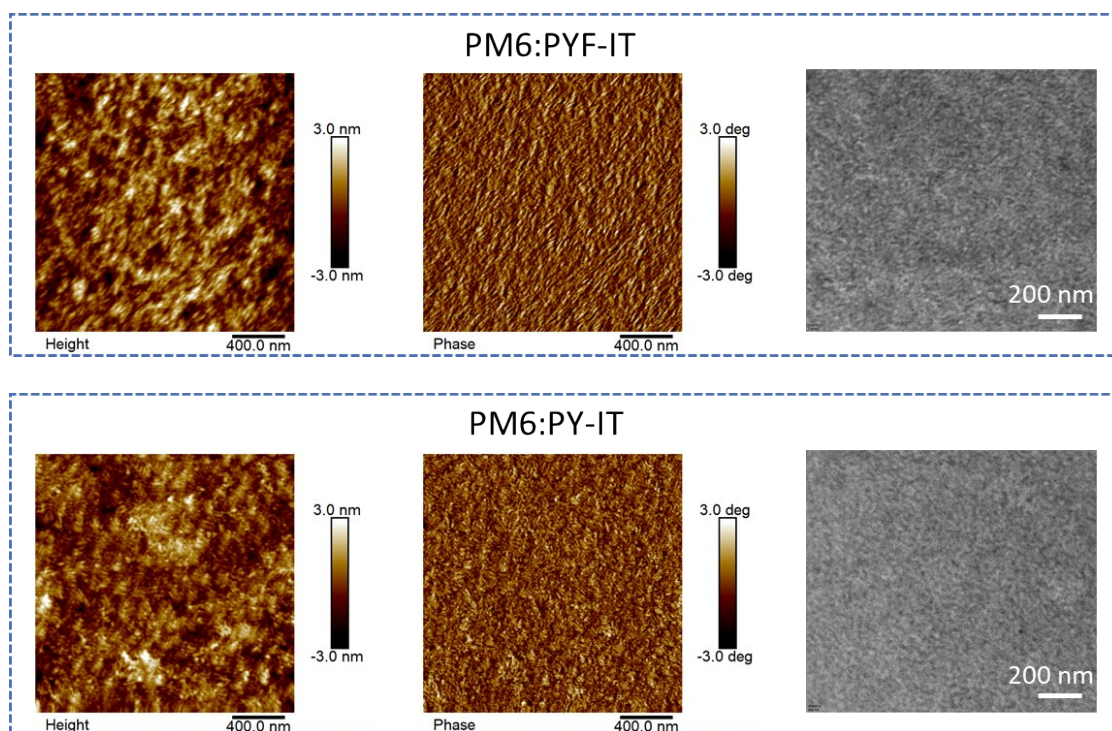
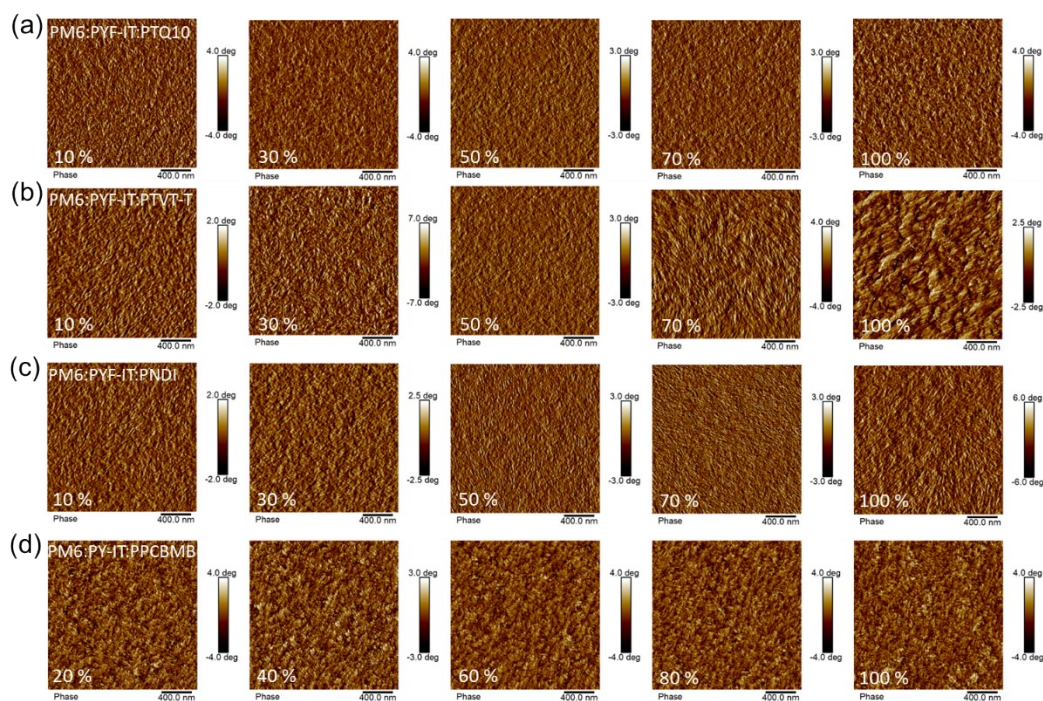Figure S4. AFM height, phase images and TEM images of PM6:PYF-IT and PM6:PY-IT.



Figure S5. AFM phase images of PM6:PYF-IT:PTQ10 (a), PM6:PYF-IT:PTVT-T (b), PM6:PYF-IT:PNDI (c) and PM6:PY-IT:PPCBMB (d) of various contents.
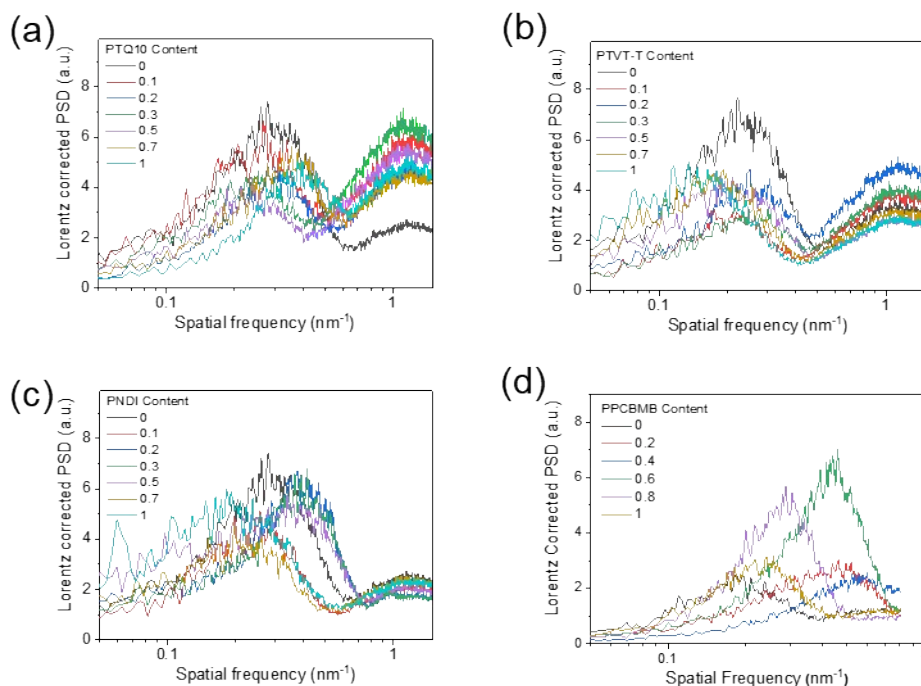
Figure S6. PSD profiles of the four polymer blends with various third component content contents. PM6:PYF-IT:PTQ10 (a) PM6:PYF-IT:PTVT-T (b) PM6:PYF-IT:PNDI (c) and PM6:PY-IT:PPCBMB (d).
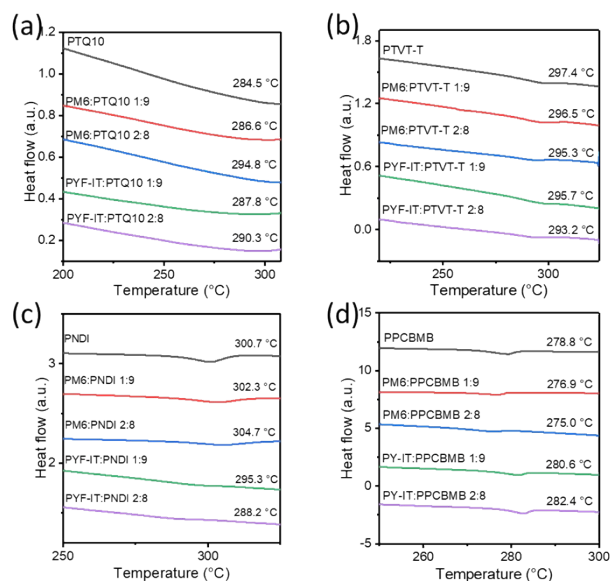


Figure S7. The melting temperature of various blend systems at different volume fractions of third component contents through DSC.

Table S7. Enthalpies of crystallization of four different blends.

| Blends | Content | Melting point (°C) | Enthalpy [$J\,g^{-1}$] |
|---|---|---|---|
| PM6:PTQ10 | 0 ： 10 | 284.5 | 1.9 |
| | 1 ： 9 | 286.6 | 2.2 |
| | 2 ： 8 | 294.8 | 1.6 |
| PYF-IT:PTQ10 | 0 ： 10 | 284.5 | 1.9 |
| | 1 ： 9 | 287.8 | 1.5 |
| | 2 ： 8 | 290.3 | 1.2 |
| PM6:PTVT-T | 0 ： 10 | 297.4 | 3.7 |
| | 1 ： 9 | 296.5 | 2.9 |
| | 2 ： 8 | 295.3 | 1.3 |
| PYF-IT:PTVT-T | 0 ： 10 | 297.4 | 3.7 |
| | 1 ： 9 | 295.7 | 3.1 |
| | 2 ： 8 | 293.2 | 2.5 |
| PM6:PNDI | 0 ： 10 | 300.7 | 5.6 |
| | 1 ： 9 | 302.3 | 5.4 |
| | 2 ： 8 | 304.7 | 5.1 |
| PYF-IT:PNDI | 0 ： 10 | 300.7 | 5.6 |
| | 1 ： 9 | 295.3 | 3.1 |
| | 2 ： 8 | 288.2 | 2.2 |
| PM6:PPCBMB | 0 ： 10 | 278.8 | 5.5 |
| | 1 ： 9 | 276.9 | 6.0 |

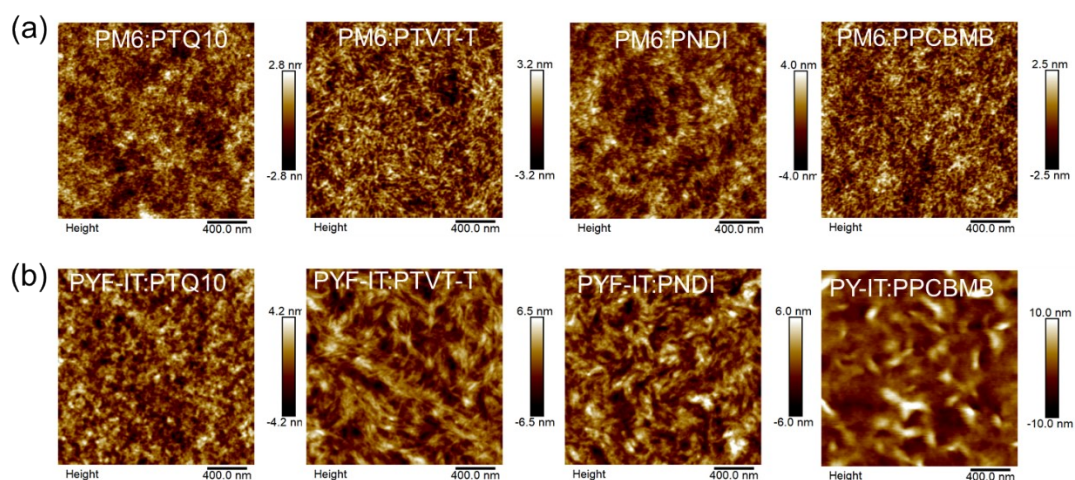| | 2：8 | 275.0 | 3.4 |
|---|---|---|---|
| | 0：10 | 278.8 | 5.5 |
| PY-IT:PPCBMB | 1：9 | 280.6 | 5.6 |
| | 2：8 | 282.4 | 6.2 |



Figure S8. AFM height images of four third component blends with polymer donor PM6 (a) and polymer acceptor PYF-IT/PY-IT (b).
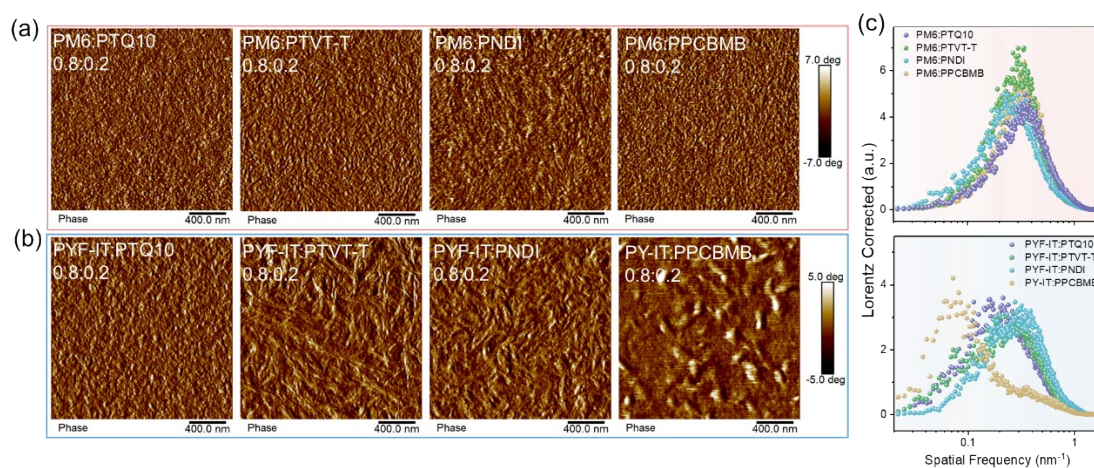


Figure S9. (a) AFM phase images of four third component blends with polymer donor PM6. (b) AFM phase images of third component blended with polymer acceptors PYF-IT/PY-IT. (c) PSD analysis of AFM phase images.
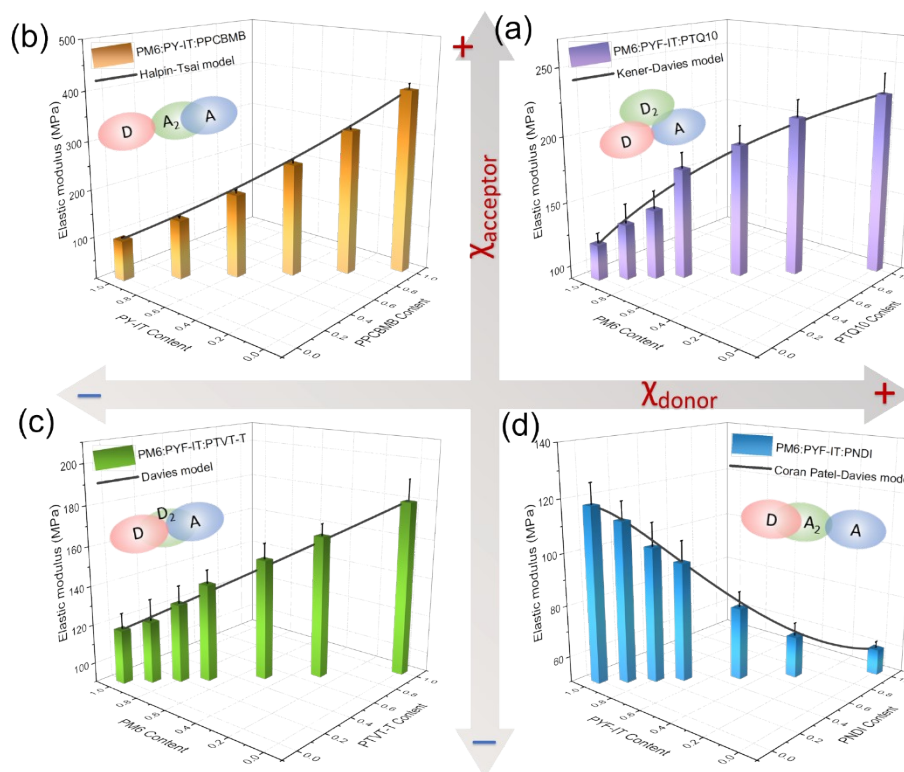
Figure S10. (a) Elastic modulus measured by FOW and Kerner-Davies model of PM6:PYF-IT:PTQ10 in Quadrant I. (b) Elastic modulus measured by FOW and Halpin-Tsai model of PM6:PY-IT:PPCBMB in Quadrant II. (c) Elastic modulus measured by FOW and Davies model of PM6:PY-IT:PTVT-T in Quadrant III. (d) Elastic modulus measured by FOW and Coran Patel-Davies model of PM6:PYF-IT:PNDI in Quadrant IV.
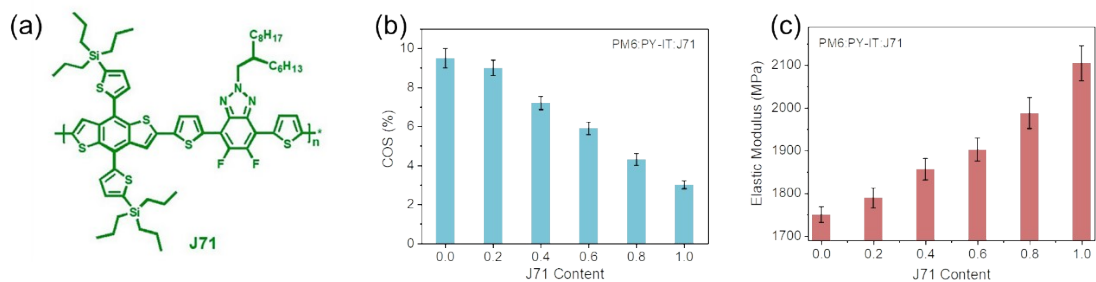


Figure S11. (a) Chemical structures of J71. The COS (b) and elastic moduli (c) of PM6:PY-IT:J71 as a function of the J71 content.

Reference

1. Davies, W.E.A. (1971). The elastic constants of a two-phase composite material. J. Phys. D: Appl. Phys. *4*, 1176.

2. Kerner, E.H. (1956). The Elastic and Thermo-elastic Properties of Composite Media. Proc. Phys. Soc. B *69*, 8.

3. Kim, J., Noh, J., Choi, H., Lee, J., and Kim, T. (2017). Mechanical Properties of Polymer–Fullerene Bulk Heterojunction Films: Role of Nanomorphology of Composite Films. Chem. Mater. *29*, 3954-3961.

4. Affdl, J.C.H., and Kardos, J.L. (1976). The Halpin-Tsai equations: A review. Polym. Eng. Sci. *16*, 344-352.

5. Coran, A.Y., and Patel, R. (1981). Rubber-Thermoplastic Compositions. Part III. Predicting Elastic Moduli of Melt Mixed Rubber-Plastic Blends. Rubber Chem. Technol. *54*, 91-100.

6. Coran, A.Y., and Patel, R. (1976). Predicting elastic moduli of heterogeneous polymer compositions. J. Appl. Polym. Sci. *20*, 3005-3016.

7. Peng, Z., Xian, K., Cui, Y., Qi, Q., Liu, J., Xu, Y., Chai, Y., Yang, C., Hou, J., Geng, Y., and Ye, L. (2021). Thermoplastic Elastomer Tunes Phase Structure and Promotes Stretchability of High-Efficiency Organic Solar Cells. Adv. Mater. *33*, 2106732.

8. Zhang, K., Xia, R., Fan, B., Liu, X., Wang, Z., Dong, S., Yip, H.L., Ying, L., Huang, F., and Cao, Y. (2018). 11.2% All-Polymer Tandem Solar Cells with Simultaneously Improved Efficiency and Stability. Adv. Mater. *30*, 1803166.

9. Kim, T., Choi, J., Kim, H.J., Lee, W., and Kim, B.J. (2017). Comparative Study of Thermal Stability, Morphology, and Performance of All-Polymer, Fullerene–Polymer, and Ternary Blend Solar Cells Based on the Same Polymer Donor. Macromolecules *50*, 6861-6871.

10. Kwon, N.Y., Park, S.H., Kang, H., Kim, Y.U., Chau, H.D., Harit, A.K., Woo, H.Y., Yoon, H.J., Cho, M.J., and Choi, D.H. (2021). Improved Stability of All-Polymer Solar Cells Using Crosslinkable Donor and Acceptor Polymers Bearing Vinyl Moieties in the Side-Chains. ACS Appl. Mater. Interfaces *13*, 16754−16765.

11. Rodríguez-Martínez, X., Riera-Galindo, S., Aguirre, L.E., Campoy-Quiles, M., Arwin, H., and Inganäs, O. (2022). Laminated Organic Photovoltaic Modules for Agrivoltaics and Beyond: An Outdoor Stability Study of All-Polymer and Polymer:Small Molecule Blends. Adv. Funct. Mater., https://doi.org/10.1002/adfm.202213220.

12. Fan, Q., Su, W., Chen, S., Liu, T., Zhuang, W., Ma, R., Wen, X., Yin, Z., Luo, Z., Guo, X., et al. (2020). A Non-Conjugated Polymer Acceptor for Efficient and Thermally Stable All-Polymer Solar Cells. Angew. Chem. Int. Ed. *59*, 19835-19840.

13. Lee, J.W., Sun, C., Ma, B.S., Kim, H.J., Wang, C., Ryu, J.M., Lim, C., Kim, T.S., Kim, Y.H., Kwon, S.K., and Kim, B.J. (2020). Efficient, Thermally Stable, and Mechanically Robust All-Polymer Solar Cells Consisting of the Same Benzodithiophene Unit-Based Polymer Acceptor and Donor with High Molecular Compatibility. Adv. Energy Mater. *11*, 2003367.

14. Lin, Z., Zhang, L., Tu, S., Wang, W., and Ling, Q. (2020). Highly thermally stable all-polymer solar cells enabled by photo-crosslinkable bromine-functionalized polymer donors. Solar Energy *201*, 489-498.

15. Su, W., Meng, Y., Guo, X., Fan, Q., Zhang, M., Jiang, Y., Xu, Z., Dai, Y., Xie, B., Liu, F., et al. (2018). Efficient and thermally stable all-polymer solar cells based on a fluorinated wide-bandgap polymer donor with high crystallinity. J. Mater. Chem. A *6*, 16403-16411.

16. Li, Z., Liang, Y., Chen, L., Chen, J., Peng, F., and Ying, L. (2023). Guest electron-accepting polymer doping enables green solvent-processed all-polymer solar cells with 16.37% efficiency. Chem. Eng. J. *452*, 139228.

17. Xian, K., Zhou, K., Li, M., Liu, J., Zhang, Y., Zhang, T., Cui, Y., Zhao, W., Yang, C., Hou, J., et al. (2023). Simultaneous Optimization of Efficiency, Stretchability, and Stability in All-Polymer Solar Cells via Aggregation Control. Chin. J. Chem. *41*, 159—166.

18. Wang, Y., Yu, H., Wu, X., Zhao, D., Zhang, S., Zou, X., Li, B., Gao, D., Li, Z., Xia, X., et al. (2022). Boosting the Fill Factor through Sequential Deposition and Homo Hydrocarbon Solvent toward Efficient and Stable All-Polymer Solar Cells. Adv. Energy Mater. *12*, 2202729.

19. Ma, R., Fan, Q., Dela Pena, T.A., Wu, B., Liu, H., Wu, Q., Wei, Q., Wu, J., Lu, X., Li, M., et al. (2023). Unveiling the Morphological and Physical Mechanism of Burn-in Loss Alleviation by Ternary Matrix Towards Stable and Efficient All-Polymer Solar Cells. Adv. Mater. *https://doi.org/10.1002/adma.202212275*.

20. Ma, L., Cui, Y., Zhang, J., Xian, K., Chen, Z., Zhou, K., Zhang, T., Wang, W., Yao, H., Zhang, S., et al. (2022). High-Efficiency and Mechanically Robust All-Polymer Organic Photovoltaic Cells Enabled by Optimized Fibril Network Morphology. Adv. Mater. *https://doi.org/10.1002/adma.202208926*.

21. Chen, Q., Han, Y.H., Franco, L.R., Marchiori, C.F.N., Genene, Z., Araujo, C.M., Lee, J.W., Phan, T.N., Wu, J., Yu, D., et al. (2022). Effects of Flexible Conjugation-Break Spacers of Non-Conjugated Polymer Acceptors on Photovoltaic and Mechanical Properties of All-Polymer Solar Cells. Nanomicro Lett *14*, 164.

22. Liu, J., Deng, J., Zhu, Y., Geng, X., Zhang, L., Jeong, S.Y., Zhou, D., Woo, H.Y., Chen, D., Wu, F., and Chen, L. (2023). Regulation of Polymer Configurations Enables Green Solvent-Processed Large-Area Binary All-Polymer Solar Cells With Breakthrough Performance and High Efficiency Stretchability Factor. Adv. Mater. *35*, e2208008.

23. Wang, J., Cui, Y., Xu, Y., Xian, K., Bi, P., Chen, Z., Zhou, K., Ma, L., Zhang, T., Yang, Y., et al. (2022). A New Polymer Donor Enables Binary All-Polymer Organic Photovoltaic Cells with 18% Efficiency and Excellent Mechanical Robustness. Adv. Mater. *34*, 2205009.

24. Kim, W., Choi, J., Kim, J.-H., Kim, T., Lee, C., Lee, S., Kim, M., Kim, B.J., and Kim, T.-S. (2018). Comparative Study of the Mechanical Properties of All-Polymer and Fullerene–Polymer Solar Cells: The Importance of Polymer Acceptors for High Fracture Resistance. Chem. Mater. *30*, 2102-2111.

25. Lee, J.-W., Ma, B.S., Choi, J., Lee, J., Lee, S., Liao, K., Lee, W., Kim, T.-S., and Kim, B.J. (2019). Origin of the High Donor–Acceptor Composition Tolerance in Device Performance and Mechanical Robustness of All-Polymer Solar Cells. Chem. Mater. *32*, 582-594.

26. Kim, T., Kim, J.H., Kang, T.E., Lee, C., Kang, H., Shin, M., Wang, C., Ma, B., Jeong, U., Kim, T.S., and Kim, B.J. (2015). Flexible, highly efficient all-polymer solar cells. Nat. Commun. *6*, 8547.